

High Density Mesoscopic Atom Clouds in a Holographic Atom Trap

J. Sebby-Strabley, R. T. R. Newell,* J. O. Day, E. Brekke, and T. G. Walker
Department of Physics, University of Wisconsin-Madison, Madison, Wisconsin 53706

We demonstrate the production of micron-sized high density atom clouds of interest for mesoscopic quantum information processing. We evaporate atoms from 60 μK , 3×10^{14} atoms/cm³ samples contained in a highly anisotropic optical lattice formed by interfering diffracted beams from a holographic phase plate. After evaporating to 1 μK by lowering the confining potential, in less than a second the atom density reduces to 8×10^{13} cm⁻³ at a phase space density approaching unity. Adiabatic recompression of the atoms then increases the density to levels in excess of 1×10^{15} cm⁻³. The resulting clouds are typically 8 μm in the longest dimension. Such samples are small enough to enable mesoscopic quantum manipulation using Rydberg blockade and have the high densities required to investigate new collision phenomena.

PACS numbers: 32.80.Pj, 39.25.+k, 39.10.+j

Two of the most important themes in current studies of ultracold incoherent matter are studies of plasmas and Rydberg atoms at low temperature and high density, and use of mesoscopic samples for topics in quantum information processing. Even at the relatively modest 10^{12} cm⁻³ densities of standard magneto-optical traps, a wide variety of new phenomena have been observed by exciting atoms near the ionization limit[1]. Similarly, the use of atomic ensembles with their collectively enhanced light-atom interactions have led to new developments such as collective spin squeezing [2], quantum memory [3], and single-photon generation[4]. With these contexts in mind we report in this Letter new techniques for producing high density ($> 10^{15}$ cm⁻³) mesoscopic (5-10 μm) samples ideal for use in both types of experiments.

In the context of high densities, we note that the recent predictions of novel ultralong range Rydberg molecular states [5, 6, 7] require extremely high densities to attain significant production rates. These “trilobite” molecules arise from the Fermi point-like interactions between Rydberg and ground-state atoms. At the densities reported here, the Fermi shifts of the Rydberg levels are on the order of 100 MHz. Similarly, the production of cold plasmas and Rydberg gases at these densities promises to reveal new phenomena not accessible in conventional laser traps which have 100-1000 times lower densities.

Regarding mesoscopic atom samples, Lukin *et al.* [8] recently proposed manipulating quantum information using the very long range dipole-dipole interactions produced by Rydberg atoms. In brief, the excitation of a single Rydberg atom strongly suppresses the excitation of other atoms within its range of influence. If the size of a sample of atoms is less than the blockade range R , then the accessible quantum states of the ensemble are limited to states of zero or one atom excitations. Using Rydberg states as intermediate states in Rabi manipulation of two hyperfine ground states then allows the production of stable but highly entangled collective excitations of the ensembles. For MHz rate quantum manipulations with cw lasers the value of R required is a few μm at principal

quantum numbers $n > 50$ [9]. The clouds produced in this experiment reach this length scale.

Recent experiments have demonstrated dramatic suppression of pulsed Rydberg state excitation in magneto-optical traps of size $L \gg R$ [10, 11]. In these experiments, the number of excited Rydberg atoms saturates at fluence values much less than expected for isolated atoms due to the Rydberg-Rydberg interactions shifting atoms out of resonance with the exciting lasers. If the Rydberg blockade is effective, the number of excited atoms should be limited to roughly $(L/R)^3$. If the blockade is not complete, saturation still occurs but with a greater number of excited atoms. Thus to differentiate blockade and suppression requires production of mesoscopic samples of size $L \sim R$ [12].

In this Letter we present a method for producing high density elliptical mesoscopic atom samples with semi-major axes σ on the order of R using rapid evaporative cooling of ⁸⁷Rb atoms from a Holographic Atom Trap (HAT), followed by adiabatic recompression. We demonstrate densities in excess of 10^{15} cm⁻³, the highest cold atom densities attained for incoherent matter. The recompression stage can produce clouds of radius as small as 5.6 μm , sufficiently small to be sensitive to single atom Rydberg blockade.

The HAT, described in detail elsewhere [13], is a lattice of interference fringes produced by imaging 5 diffracted orders (zeroth order plus 4 equal intensity first order beams) from a holographic phase plate. The laser used is an 18W cw flashlamp-pumped Nd:YAG laser at 1.064 μm , intensity stabilized and controlled using an acousto-optic modulator feedback system. Along the propagation axis the Talbot effect gives rise to a series of interference fringes. Each Talbot fringe contains a lattice with a unit cell of 10 $\mu\text{m} \times 10 \mu\text{m} \times 100 \mu\text{m}$ as illustrated in Figure 1. The five diffracted orders are focussed to approximately 90 μm waists at the region of intersection, giving a typical full-intensity trap depth of $U_0 = 600 \mu\text{K}$, and trap oscillation frequencies of 18.4 ± 1.2 kHz, 18.4 ± 1.2 kHz, and 735 ± 62 kHz. Atoms are loaded into the HAT from

a forced-dark-spot $F = 1$ magneto-optical trap [14].

We use absorption imaging to characterize the spatial distribution of the atoms in the HAT, to make absolute measurements of the number of atoms, and to measure the atomic temperature via time-of-flight techniques. The HAT is first turned off in $10 \mu\text{s}$ in order to eliminate AC Stark shifts and excited state hyperfine mixing. Then a $150 \mu\text{s}$ pulse of light from a diode laser tuned to the $5S_{1/2}(F = 1) \rightarrow 5P_{1/2}(F' = 2)$ transition passes through the atoms which are imaged onto a CCD camera. The imaging lens system is a pair of commercial achromats that give an aberration-limited resolution of approximately $5 \mu\text{m}$. Images are analyzed to deduce the number and distribution of atoms contained in the different microtraps. We make use of a calibrated absorption method for absolute number measurements [15]. When the fluence of the imaging pulse is sufficient to remove all the atoms from the $F = 1$ state, the average number of photons absorbed per atom is given simply from the fluorescence branching ratios to be 2. The number of atoms is then directly determined from the camera quantum efficiency and the transmission of the lenses. For small numbers of atoms and for time-of-flight temperature measurements, an additional laser tuned to repump the atoms back to $F = 1$ can be used to artificially increase the number of photons absorbed per atom.

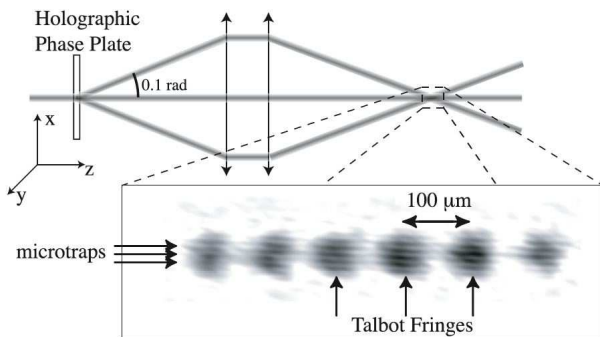


FIG. 1: Holographic Atom Trap: five laser beams diffracted from a phase plate are imaged onto a MOT cloud. Atoms collect in the intensity maxima of the interference pattern of the beams.

After loading atoms into the HAT at densities of $3 \times 10^{14} \text{ cm}^{-3}$ and temperatures of $60 \mu\text{K}$, the atoms are distributed over typically five Talbot fringes, with each Talbot fringe containing typically 25 occupied microtraps of slightly differing trap depths. Atoms in these microtraps have sufficiently high collision rates (20,000/s) to initiate forced evaporative cooling. Using established protocols [16, 17], we gently reduce the HAT intensity, allowing high kinetic energy atoms to escape while retaining low energy atoms and thereby increasing phase space density. The evaporation process tightly couples the trap depth U and the temperature so that $T \approx U/10$. During

evaporation, the density n scales as the atom number N ; the phase space density ρ scales as $N\nu^3/T^3 \propto n/U^{3/2}$. Even though the density and the collision rates decrease with time, they are sufficiently high in the HAT that the limit on the evaporation speed is the required adiabaticity of the z-motion and the desire not to remove too many atoms. An interesting feature of the HAT is the inequivalence of the various trapping sites: sites towards the edge of the trap are more weakly bound than those at the center. As the evaporation proceeds atom loss from the outer sites is greater, causing the fraction of atoms contained in the central microtrap to increase from initially 6% to nearly 15%. Atom densities and phase space densities as a function of time are shown in Figure 2.

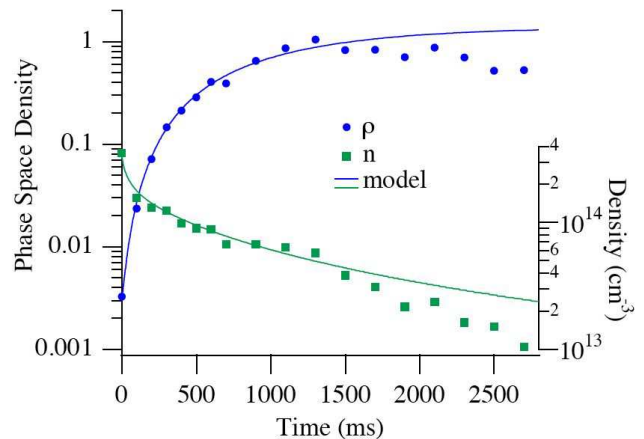


FIG. 2: During forced evaporation the phase space density ρ approaches unity while the density n decreases with atom loss.

After evaporating to a final temperature T_e and density n_e , typically $1 \mu\text{K}$ and $8 \times 10^{13} \text{ cm}^{-3}$, we recompress the cloud by adiabatically returning the trap depth to its maximum value U_0 . Since the trap depth increases more rapidly than the temperature, this shuts off evaporation, holding the number of atoms constant in the absence of loss mechanisms. The phase space density is conserved for an adiabatic process, thus $T \propto \nu \propto U^{1/2}$ and $n \propto N\nu^3/T^{3/2}$. As a result, the recompressed density is $n_r = n_e(U_0/U_e)^{3/4}$. In our case, this gives a factor of 20 density increase, consistent with our measured final density of $1.8 \pm 0.5 \times 10^{15} \text{ cm}^{-3}$.

A simple argument shows that the final attainable density using this method depends not only on the phase space density ρ_e achieved from evaporation, but the temperature T_e as well. The density n_e after evaporation is proportional to the product $\rho_e T_e^{3/2}$. The compression factor is $(U_0/U_e)^{3/4} \propto T_e^{-3/4}$ for fixed U_0 , hence the highest density is achieved when evaporating to a U_e which maximizes the function $\rho_e T_e^{3/4}$ (see inset to Fig. 3). Continuing to lower U_e does not achieve higher densities. Evaporating to lower trap depths takes in-

creasingly more time due to the adiabatic constraints. Losses from heating mechanisms and background collisions cause $\rho_e T_e^{3/4}$ to slowly decrease. This effectively determines the optimum value of U_e at which to start the recompression. Even with this constraint on U_e it is interesting to point out the wide range of densities attainable with this method.

We show recompression data for various values of U_e in Figure 3. Like evaporation, the limiting timescale for recompression is adiabaticity. However, unlike evaporation, the number of atoms is conserved so the potential can be ramped up rapidly. Figure 3 shows that even at the lowest values of U_e densities over 10^{15} cm^{-3} can be achieved in less than 900 ms. The adiabatic constraints on the $U_e = 10 \text{ } \mu\text{K}$ data in Figure 3 were purposely lightened to limit losses due to background collisions and heating mechanisms. The effect is a small breakdown of the scaling ratios which assume perfect adiabaticity.

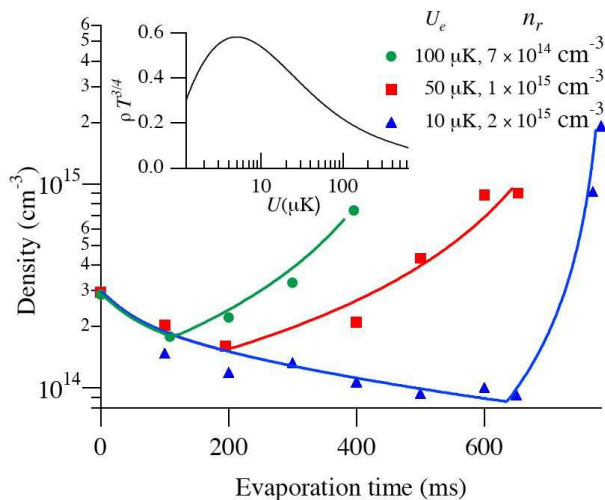


FIG. 3: Compression data and model (solid line) for 3 values of U_e . The inset shows how the key parameter $\rho T^{3/4}$ varies with trap depth.

The high densities are deduced from measurements of the number of atoms, the fraction of atoms in each microtrap, the temperature, and direct measurements of the trap spring constants. The latter are obtained using the parametric heating method [18]. We confirm the inferred densities using measurements of known 3-body recombination rates and by imaging the z-axis spatial distribution. The three-body recombination rates are determined by measuring the number of atoms in the recompressed central microtrap as a function of time after recompression: $dN/dt = -K \int n(t)^3 dV - \Gamma N$, where K is the 3-body recombination rate coefficient and Γ the loss rate due to background collisions. Data are shown in Figure 4. After recompression the temperature is too small to allow evaporation. However, heating mechanisms in-

crease the temperature with time. As a result, $n(t)$ decreases due to both recombination losses and temperature increases. Taking these effects into account, we find $K = 3.5 \pm 1.9 \times 10^{-29} \text{ cm}^6/\text{s}$, in close agreement with previous measurements [19, 20]. We have measured the rate in a magnetic field of 2.5 Gauss typically present in magnetic traps. At this field we measure $K = 4.8 \pm 2.3 \times 10^{-29} \text{ cm}^6/\text{s}$. These results are extremely sensitive to density errors; the agreement with previous experiments is confirmation of the reliability of the density measurements.

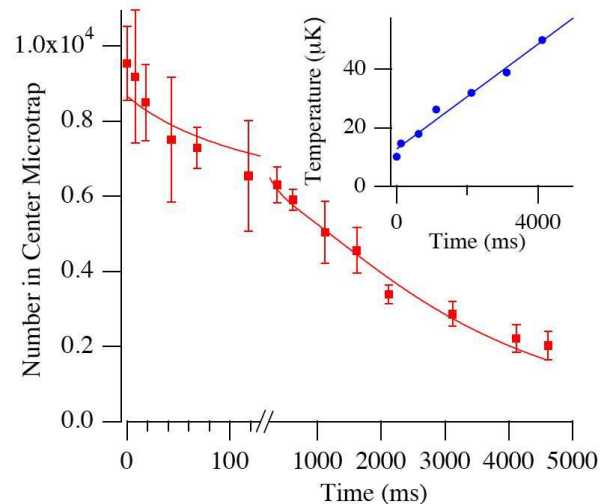


FIG. 4: After recompression we observe rapid atom loss due to 3-body recombination. Since there is no evaporation from the recompressed clouds we can measure trap heating rates by directly measuring dT/dt (inset).

We have also confirmed the densities by measuring cloud sizes. After evaporation and recompression, the semi-minor axis of the cloud is only 430 nm, too small to optically resolve. However, the z-axis size of $10.8 \text{ } \mu\text{m}$ at $13 \text{ } \mu\text{K}$ is resolvable. The measured z-axis sizes agree to within 0.5 microns with the value $\sigma = \sqrt{2T/m\omega^2}$ expected from the frequency and temperature measurements, once optical resolution and motion of the atoms during the imaging pulse are taken into account.

In addition to using evaporation followed by recompression to produce high densities, it can be used to produce strong confinement of the atoms. During evaporation, the spatial dimensions σ of the atom clouds are unchanged since both T and ω^2 scale linearly with trap depth. During recompression $T \propto \omega$ so that $\sigma \propto (U_0/U_b)^{1/4}$ yields up to a factor of 4 in size reduction for trap depth ratios of 300 that we have produced in our system. The smallest clouds we can directly observe are inferred from this ratio and the measured trap depth of $2 \text{ } \mu\text{K}$ to be $\sigma = 5.6 \text{ } \mu\text{m}$. The smallest clouds for which we have a direct temperature measurement have $\sigma = 8 \text{ } \mu\text{m}$.

We now evaluate these results in the context of Ry-

berg blockade. We imagine excitation to ns Rydberg states with a Gaussian beam of waist $10\ \mu\text{m}$. For non-uniform excitation, the appropriate figure of merit is the Rydberg-Rydberg level shift $\bar{\Omega}$ defined via $1/\bar{\Omega}^2 = \langle |1/\Omega_{ij}|^2 \rangle$ averaged over all atom pairs ij . Using calculated ns-ns potentials [9] with $n = (70, 95)$, we find $\bar{\Omega} = (2.0, 62)$ MHz for $\sigma = 5.6\ \mu\text{m}$, and $\bar{\Omega} = (0.7, 21)$ MHz for $\sigma = 8.0\ \mu\text{m}$. For a collective $2\ \mu\text{s}$ π -pulse, the probability of double excitation even in the worst case of $\bar{\Omega} = 0.7$ MHz is 6%. Thus these clouds are extremely well-suited to investigate high speed, high fidelity collective coherent quantum manipulations.

For some applications, it may be useful to isolate a single microtrap from the others. To do this, we exploit the anisotropy of the microtraps to parametrically heat the atoms in the outer microtraps with little disturbance to the atoms contained in the central microtrap. The quality factor for our parametric heating experiment is about 10 for the x-direction, sufficient to give significant differentiation of the 3% difference in oscillation frequencies between the center and outer microtraps. Thus we drive the parametric resonance at its low frequency tail, selectively heating and ejecting the atoms from the outer microtraps while causing minor heating for the center microtrap. Doing this, we have been able to increase the center well fraction from 15% to above 40%.

In addition to its utility for generating high densities and small clouds, adiabatic recompression also allows direct measurements of trap heating rates. Under conditions of evaporation, heating mechanisms do not actually increase the temperature when evaporation is rapid enough to recool the atoms by atom loss. Thus heating and loss mechanisms can be difficult to disentangle under conditions of evaporation. However, evaporation no longer functions after recompression, and heating rates can be deduced directly from measured temperature increases with time. Example data are shown in the inset to Figure 4. The deduced heating rate $dE/dt = 3dT/dt$ is a factor of 1.4 larger than the predictions of Bali *et al.* [21] for quantum diffractive heating. Indeed, taking this measured heating rate into account in our evaporation model, combined with the heating due to multiple scattering as predicted by Beijerinck [22], we generate the solid curve in Fig. 2 that accounts for our measured phase space density as a function of time.

The experiments we have described represent a robust method for producing the kinds of high density ($> 10^{15}\ \text{cm}^{-3}$) and small size clouds ($< 8\ \mu\text{m}$) of interest for Rydberg atom studies both in the high density regime of ultracold plasmas and molecular spectroscopy, and in the small size regime relevant to coherent single-atom ma-

nipulation for quantum information processing. Many other proposed applications, including deterministic single atom and photon sources [23] and fast quantum state detection and transmission schemes [24], require these types of sources for their operation.

This work was supported by the NSF and NASA. We appreciate discussions with M. Saffman, C. Greene, B. Esry, J. Thomas and H. Beijerinck.

* Current address: LANL

- [1] C. Simien *et al.*, Phys. Rev. Lett. **92**, 143001 (2004); T. Pohl, T. Pattard, and J. M. Rost, Phys. Rev. Lett. **92**, 155003 (2004); A. Walz-Flannigan, J. Guest, J.-H. Choi, and G. Raithel, Phys. Rev. A **69**, 634051 (2004); T. Gallagher *et al.*, J. Opt. Sci. Amer. B **20**, 1091 (2003); J. L. Roberts, C. F. Fertig, M. L. Lim, and S. L. Rolston, physics/040204 (2004).
- [2] J. Hald, J. L. Sorensen, C. Schori, and E. S. Polzik, Phys. Rev. Lett. **83**, 1319 (1999); A. Kuzmich, L. Mandel, and N. P. Bigelow, Phys. Rev. Lett. **85**, 1594 (2000).
- [3] C. H. van der Wal *et al.*, Science **301**, 196 (2003).
- [4] C. W. Chou, S. V. Polyakov, A. Kuzmich, and H. J. Kimble, Phys. Rev. Lett. **92**, 213601 (2004).
- [5] C. H. Greene, A. S. Dickinson, and H. R. Sadeghpour, Phys. Rev. Lett. **85**, 2458 (2000).
- [6] C. Boisseau, I. Simbotin, and R. Cote, Phys. Rev. Lett. **88**, 133004 (2002).
- [7] S. Farooqi *et al.*, Phys. Rev. Lett. **91**, 183002 (2003).
- [8] M. D. Lukin *et al.*, Phys. Rev. Lett. **87**, 37901 (2001).
- [9] T. G. Walker and M. Saffman, physics/0407048 (2004).
- [10] D. Tong *et al.*, physics/0402113 (2004).
- [11] K. Singer *et al.*, physics/0402113 (2004).
- [12] An additional requirement is that the Rydberg-Rydberg interaction has no dipole-dipole zeros. See Ref. [9].
- [13] R. Newell, J. Sebby, and T. Walker, Opt. Lett. **28**, 1266 (2003).
- [14] M. H. Anderson, W. Petrich, J. R. Ensher, and E. A. Cornell, Phys. Rev. A **50**, R3597 (1994).
- [15] K. E. Gibble, S. Kasapi, and S. Chu, Opt. Lett. **17**, 526 (1992).
- [16] K. Davis, M.-O. Mewes, and W. Ketterle, Appl. Phys. B **60**, 155 (1995).
- [17] K. M. O'Hara, M. E. Gehm, S. R. Granade, and J. E. Thomas, Phys. Rev. A **64**, 51403 (2001).
- [18] S. Friebe *et al.*, Appl. Phys. B **B67**, 699 (1998).
- [19] E. A. Burt *et al.*, Phys. Rev. Lett. **79**, 337 (1997).
- [20] B. L. Tolra *et al.*, Phys. Rev. Lett. **92**, 190401 (2004).
- [21] S. Bali *et al.*, Phys. Rev. A **60**, R29 (1999).
- [22] H. C. W. Beijerinck, Phys. Rev. A **62**, 63614 (2000).
- [23] M. Saffman and T. G. Walker, Phys. Rev. A **66**, 65403 (2002).
- [24] M. Saffman and T. G. Walker, quant-ph/0402111 (2004).